Validation for Ice Flow Velocity Variations of Shirase Glacier Derived From PALSAR-2 Offset Tracking

Kazuki Nakamura, *Member, IEEE*, Shigeru Aoki, Tsutomu Yamanokuchi, Takeshi Tamura, and Koichiro Doi

***Abstract*—We have shown that the flow velocity of Shirase Glacier can be estimated by applying the offset tracking method to the amplitude images derived from the phased array type L-band synthetic aperture radar type-2 (PALSAR-2) onboard the Advanced Land Observing Satellite-2. Although the offset tracking is widely used, the method is sometimes not applicable effectively and the reason is not always clear. Here, we consider a possibility of ionospheric contamination and show the validation results of the estimated flow velocity applied the offset tracking method to the PALSAR-2 data, based on *in-situ* measurement of the flow velocity from the GNSS receiver on the autonomous phase-sensitive radio echo sounder simultaneously with the PALSAR-2 observation. As a result, the ionospheric contamination can yield a spurious error of $\pm$0.2 km a^{-1}. After statistically removing the erroneous pairs, the RMSE was 0.049 km a^{-1} derived from the flow velocity error between the *in-situ* measurement results and estimated from satellite, and the estimated flow velocity obtained using PALSAR-2 data is proved to be in good agreement with the ground truth. Obtained spatial and temporal variations reveal signature of glacier dynamics, which prove the efficacy of the offset tracking method. The obtained ice-flow velocity increases rapidly from the upstream region to the coast, but its velocity is roughly constant over a region, 10-km long about the grounding line (GL), then gradually tends to increase again downstream from the GL. This trend has continued largely unchanged over 24 years since 1996.**

***Index Terms*—Advanced Land Observing Satellite-2 (ALOS-2), autonomous phase-sensitive radio echo sounder (ApRES), flow velocity, phased array type L-band synthetic aperture radar type-2 (PALSAR-2), Shirase Glacier.**

I. Introduction

AS THE global average temperature continues to rise, there is an urgent need to investigate the global mass transfer associated with water phase changes, and the rise in sea level associated with the melting of ice stored on land is great social concern. Water exists on the earth is approximately 1.4 $\times$ 10^9 km^3 within seawater of approximately 98%. The remaining water, i.e., water on land, is stored as ice in ice sheets of approximately 70% [1]. Annual snowfall on the Antarctic ice sheet (accumulation) is estimated to be 5 mm in terms of sea level height [2], and estimated ice discharge for major glaciers only is 2.3 mm a^{-1} [3]. Although a very small difference between ice accumulation and discharge relative to the total ice sheet volume has been discussed, no definitive estimates are currently available. However, this small difference has a significant impact on the annual sea level change.

In recent years, the glacier flow velocity has been rapidly increasing in West Antarctica due to the basal melting of ice shelves. The mass balance, which is the sum of snow accumulation in the ice sheet and ice discharge by runoff to the ocean, tends to be negative such that the amount of ice discharge exceeds that of accumulation [4]. On the other hand, the mass balance of the ice sheet in East Antarctica has been considered to be nearly balanced [5], [6]. This is because almost all of West Antarctica has the bedrock elevation below sea level of –440 m, while that in East Antarctica is 15 m [7], and this has been considered as one of the factors accelerating ice discharge due to basal melting of the glacier in West Antarctica. However, the mass balance of the ice sheet in the Shirase drainage basin, which has the fastest ice stream of Shirase Glacier in East Antarctica, is estimated to be –1.9 Gt a^{-1} [8]. This suggests the negative trend of mass balance in the area around Shirase Glacier, but the interannual variation in flow velocity which dominates that trend is still insufficiently studied. In addition, basal melting of the floating ice tongue of Shirase Glacier in East Antarctica as well as West Antarctica has been reported due to the inflow of warm seawater from offshore [9].

As mentioned above, it is very important to extensively study the snow accumulation and ice discharge of glaciers and ice sheets in Antarctic regions, but until now has been discussed those fluctuations by field surveys using a triangulation method, radio positioning based on satellite Doppler observation, GPS survey, and so on [10]–[12]. The Antarctic region is not only immense area, but also has a severe weather environment, polar night, and crevasses that make field observation hazardous and difficult. A satellite remote sensing technique is to observe spatiotemporally and continuously, which is effective for that observation target in cryosphere. Optical sensors are affected by weather and solar altitude, so it is difficult to obtain observation

Manuscript received December 27, 2021; revised March 18, 2022; accepted March 30, 2022. Date of publication April 8, 2022; date of current version May 6, 2022. This work was supported in part by the MEXT Grant-in-Aid for Scientific Research on Innovative Areas under Grant 17H06321, in part by the JSPS Grant-in-Aid Scientific Research (C) under Grant 18K11627 and Grant 21K12214, in part by the Joint Research Program of the Institute of Low Temperature Science, Hokkaido University under Grant 20G040 and Grant 21G027, and in part by the NIPR through General Collaboration Project (31-23 and 2-25). *(Corresponding author: Kazuki Nakamura.)*

Kazuki Nakamura is with the College of Engineering, Nihon University, Koriyama 963-8642, Japan (e-mail: nakamura.kazuki@nihon-u.ac.jp).

Shigeru Aoki is with the Institute of Low Temperature Science, Hokkaido University, Sapporo 060-0819, Japan (e-mail: shigeru@lowtem.hokudai.ac.jp).

Tsutomu Yamanokuchi is with the Remote Sensing Technology Center of Japan, Tsukuba 305-0047, Japan (e-mail: tsutomuy@restec.or.jp).

Takeshi Tamura and Koichiro Doi are with the Inter-University Research Institute Corporation Research Organization of Information and Systems, National Institute of Polar Research, Tachikawa 190-8518, Japan (e-mail: tamura.takeshi@nipr.ac.jp; doi@nipr.ac.jp).

Digital Object Identifier 10.1109/JSTARS.2022.3165581

opportunities in the polar regions continuously as planned. Synthetic aperture radar (SAR) is an active microwave sensor and has high transparency for atmosphere. SAR illuminates microwave to the earth's surface and observes the microwaves scattered on the surface. The observation is possible even if it is during polar night, and the spatial resolution of SAR comparable to that of optical sensors.

In order to quantitatively understand the dynamics of accumulation and discharge for the glacier and ice sheet, it is necessary to accurately observe 1) the grounding line (GL) of the ice sheet, 2) the flow velocity of the glacier and ice sheet, and 3) the thickness of the ice sheet and ice shelf derived from the surface elevation. An interferometry SAR (InSAR) technique for the first time was applied to the glacier and ice sheet in Antarctica in 1993 [13]. This article which was presented as the image of glacier motions that appeared as interference fringe patterns, interferometric fringes were extracted from a pair of SAR data called the Ice Mode in European Remote sensing Satellite-1. The InSAR has also been reported to be effective in detecting a GL [14], [15] and glaciers and ice sheets as flow velocities were slow [16].

The ice flow observation of the Shirase Glacier using a remote sensing technique began with the report that the mean flow velocity in the floating ice tongue was estimated to be 2.5 km a^{-1} based on the movement of feature points on the glacier compared using two aerial photographs taken at different times [17], [18]. While InSAR results showed that the velocity distribution around the same floating ice tongue ranged 2.2–2.6 km a^{-1} [19], furthermore, the flow velocity at the GL of Shirase Glacier, which was 2.3 km a^{-1}, is one of the fastest flowing glaciers compared to other glaciers since the mean flow velocity of nine glaciers in East Antarctica was 1.0 km a^{-1} [20]. The InSAR is a technique to quantify the movement of glaciers and ice sheets on the centimeter order from measuring the phase difference of microwaves, but it is difficult to apply measuring movement with large displacement gradients because of using phase information. Specifically, if there are variations in glaciers and ice sheets in the line-of-sight direction that are larger than the half-wavelength of using microwaves at the distance between adjacent pixels, the phase difference changes by more than π caused a loss of spatial continuity in the phase difference and a decrease in correlation. In contrast, the offset tracking method uses the amplitude information to calculate directly displacements between pixels without using phase information, enabling measurements on the order of meters even in glaciers, and ice sheets with large displacement gradients.

The approach taken in matching the amplitudes of SAR images can be used in correlating scenes over a long time period, as shown by [21]. To apply the flow velocity estimation with fast ice stream of the Shirase Glacier, an offset tracking method applied to SAR amplitude images and the analysis of Japanese Earth Resources Satellite (JERS)-1/SAR data acquired between 1996 and 1998 revealed seasonal variations in the ice flow of Shirase Glacier [21]. Analysis of Advanced Land Observing Satellite (ALOS)/phased array-type L-band synthetic aperture radar (PALSAR) data acquired between 2007 and 2010 showed that the flow velocity in the upstream region varied up to 0.6 km a^{-1} over 15 years [22]. The results of the analysis of ALOS-2/PALSAR-2 data acquired from 2014 to 2015 showed that the upstream flow velocity continued to accelerate [23].

The accuracy of offset tracking method depends strongly on the accuracy of image alignment; an image matching on the subpixel order applying a two-dimensional FFT oversampling method allow alignment with a resolution less than 0.1 pixel [24]. Although the resolution can theoretically be increased without limit by increasing the oversampling factor, the potential error inherent in the offset tracking method was investigated by applying that method to SAR image pairs with no apparent displacement, and the results showed that errors related to topographic undulations and ionospheric delays were between submeter and meters order [25].

The offset tracking method has also been used to estimate the flow velocity of the Shirase Glacier, but the estimation accuracy has been dealt with one-pixel offset after image alignment [21]–[23]. However, the estimation result from the offset tracking method is necessary, for example, to compare the results of the offset tracking method with the results of field surveys on the Shirase Glacier. Recently, the 59th Japanese Antarctic Research Expedition (JARE), *in situ* measurement has been carried out with the autonomous phase-sensitive radio echo sounder (ApRES) [9] installed on the Shirase Glacier, so the flow velocities could be calculated using position data from the GNSS receiver of the ApRES (ApRES/GNSS).

This means that it is possible to validate the estimation accuracy of the flow velocity of the Shirase Glacier using the offset tracking method. This article describes the validity of estimating flow velocity applied the offset tracking method to the ALOS-2/PALSAR-2 amplitude image that was compared with the calculated flow velocity based on the ApRES/GNSS data.

II. Shirase Glacier

Shirase Glacier was named after the Japanese explorer Nobu Shirase, who explored Antarctica in the early 20th century. Shirase Glacier is located approximately 150 km south of Syowa Station (Fig. 1). The drainage basin of Shirase Glacier is located in Dronning Maud Land and forms part of the Mizuho Plateau [26], [27]. The drainage basin of the Shirase Glacier is the terminus of the ice stream of the Shirase Glacier reaches Lützow-Holm Bay in the form of a floating ice tongue (Fig. 1). Given that the floating ice tongue is surrounded by landfast ice that covers most of the Lützow-Holm Bay, the glacier mass has no direct outlet from Lützow-Holm Bay. As a result, conglomerates of icebergs form in the Lützow-Holm Bay [28].

III. Data Analysis

A. ALOS-2/PALSAR-2 Data

We employed data gathered by SAR instrumentation on the ALOS-2 satellite. The ALOS-2 satellite, which is a follow-on satellite of the ALOS, was launched on an H-II booster in 2014 by the Japanese Aerospace Exploration Agency (JAXA). The repeat cycle of ALOS-2 was 14 days and it carried an L-band

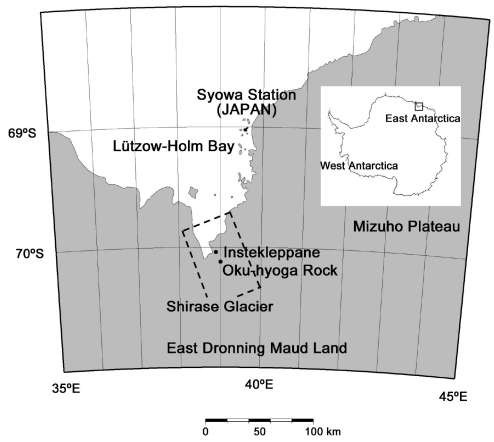

Fig. 1. Map of Lützow-Holm Bay, East Antarctica. The dashed rectangle defines the area of Shirase Glacier analyzed in the present article.

SAR (wavelength is approximately 24 cm). Since the ALOS-2 repeat cycle of 14 days is shorter than that of the ALOS (46 days), a good correlation in our analysis is expected using the ALOS-2/PASALR-2 data. Starting from 2018, the PALSAR-2 has been used to observe the Shirase Glacier which is synchronous with the observation of ApRES.

Short temporal intervals between images are preferable for the purpose of the present article because the longer the repeat cycle involved in capturing SAR images, the more likely decorrelation would occur between consecutive images due to changes in the scattering characteristics of the glacier and the ice sheet surface over time. We used a total of 20 pairs of PALSAR-2 images in 2018–2019, basically 14 days intervals, which were generated from the single-look complex data provided by the ALOS Research Announcement of JAXA (ALOS-RA). Table I lists the acquisition dates of the ALOS-2/PALSAR-2 scenes analyzed using an offset tracking. Also, specification parameters of the ALOS-2/PALSAR-2 used in this article is listed in Table II.

To compare with the results from other satellites and investigate temporal changes, previous satellites are used. The JERS-1 satellite was equipped with an L-band SAR (23.6 cm wavelength) with its repeat cycle of 44 days. The JERS-1/SAR intensively observed the area around Shirase Glacier from 1996 to the end of its operation in 1998. These data were acquired by descending orbit with HH polarization at the offnadir angle of 35°, and archived by the National Institute of Polar Research for use in the previous article [21].

The ALOS satellite has the repeat cycle of 46 days and is equipped with the PALSAR, an L-band SAR (23.5 cm wavelength), as a successor to the SAR onboard the JERS-1. In 2007–2010, the scenes including the Shirase Glacier were acquired which were provided by the ALOS-RA and used for previous article [22]. The data was acquired by the ascending orbit using the HH polarization in the fine beam single polarization (FBS) mode with the offnadir angle of 34.3°. The bandwidth of the FBS mode is approximately twice that of the JERS-1/SAR, and the resolution in the range direction (radar illumination direction) was to be improved.

TABLE I
ALOS-2/PALSAR-2 ACQUISITION DATE USED IN THIS ARTICLE

	Primary image	Secondary image
(a)	1 July 2018	12 August 2018
(b)	12 August 2018	21 October 2018
(c)	21 October 2018	4 November 2018
(d)	4 November 2018	30 December 2018
(e)	13 January 2019	27 January 2019
(f)	27 January 2019	24 February 2019
(g)	24 February 2019	10 March 2019
(h)	10 March 2019	24 March 2019
(i)	24 March 2019	7 April 2019
(j)	7 April 2019	21 April 2019
(k)	21 April 2019	5 may 2019
(l)	5 may 2019	19 May 2019
(m)	19 May 2019	2 June 2019
(n)	2 June 2019	16 June 2019
(o)	16 June 2019	30 June 2019
(p)	30 June 2019	14 July 2019
(q)	14 July 2019	28 July 2019
(r)	28 July 2019	11 August 2019
(s)	11 August 2019	25 August 2019
(t)	25 August 2019	8 September 2019

TABLE II
ALOS-2/PALSAR-2 ACQUISITION DATE USED IN THIS ARTICLE

Satellite altitude	628 km
Radar frequency	1.2 GHz (L-band)
Radar wavelength	approx. 24.0 cm
Number of looks	range 1, azimuth 2
Pixel resolution after ground range conversion	8 m (resampled)
Swath Width	approx. 70.0 km
Offnadir Angle	36.6º (beam no.2)
Polarization	HH

At the beginning of the ALOS-2/PALSAR-2 observation in 2014–2015, the scene including the Shirase Glacier was mainly acquired by the ScanSAR mode, which used to estimate the flow velocity in previous article [23]. The data was acquired by the descending orbit with the HH polarization at the offnadir angle of 26.2° in the strip of scan number 1 (the most near-range side) included the Shirase Glacier.

Based on the results of previous articles and the analysis of this article from the ALOS-2/PALSAR-2 with the fine beam mode in 2018–2019, the fluctuations of the flow velocity in the Shirase Glacier over the 24-year period can be determined, which were discussed as in Section IV-C and D.

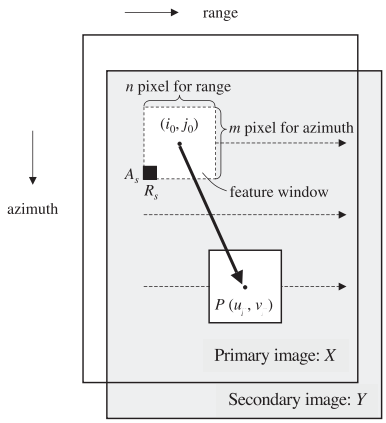

Fig. 2. Conceptual diagram of offset tracking between the primary image (white scene behind) and the secondary image (shadowed scene above). A feature window of *n* pixels for range and *m* pixels for azimuth is moved to maximize the correlation coefficient $R(u, v)$ given by (1).

B. Estimation of Ice Flow Velocity Using PALSAR-2 Data

The flow vector or the pixel offset, in the slant-range coordinate system, was obtained by applying an offset tracking method to coregistered image pairs. The purpose of the offset tracking method is to match similarity surface points in small areas extracted from an image pair. Fig. 2 shows a schematic diagram of the correlation method. The reference image is referred to as the "primary image" and the search image is referred to as the "secondary image." Small areas called "correlation windows," of *m* (azimuth) × *n* (range) pixels in size are established and are considered to be matched when the correlation coefficient, *R*, is maximized. The correlation coefficient, *R*, is calculated as follows: Eq. (1) shown at the bottom of this page where $X(i, j)$ is the pixel value at the coordinates of the primary element *X* with range *i* and azimuth *j*, and $Y(i + u, j + v)$ represents the pixel value at the secondary element *Y*, at a distance (u, v) from (i, j). $\bar{X}$ and $\bar{Y}$ represent the mean element values in a given small area consisting of *n* pixels in the range direction and *m* pixels in the azimuth direction, in the primary and secondary images, respectively.

To calculate the flow offsets derived from the pixel offsets, an area of 128 × 128 pixels in the case of ALOS-2/PALSAR-2 images correspond to about 1.05 km^2 (1.02 × 1.02 km). These size settings were selected to match the size of iceberg fragments in the offset tracking. Once the offsets, (u, v), at which *R* is maximized are determined using (1), the flow offsets, A_z and R_g, in each direction in the slant-range coordinate system can be calculated easily by (2), using the ground resolutions A_0 and R_0 for each pixel in the azimuth and range directions

$$A_z = A_0 \times v \tag{2a}$$

$$R_g = R_0 \times u. \tag{2b}$$

Here, the relationships between A_z and R_g and the northward, eastward, and upward positive displacements (U_n, U_e, and U_z) in the geographical coordinate system [29] are given by

$$A_z = \sin\theta\, U_e + \cos\theta U_n \tag{3a}$$

$$R_g = \cos\phi\, \sin\theta U_e - \sin\phi \sin\theta U_n - \cos\theta U_z. \tag{3b}$$

Using the satellite's heading angle, ϕ, measured clockwise from the north and the microwave incidence angle at the ground, θ, and approximating $U_z = 0$, each offset can be estimated as follows:

$$U_n = \cos\phi\, A_z - \left(\frac{\sin\phi}{\sin\theta}\right) R_g \tag{4a}$$

$$U_e = \sin\phi\, A_z + \left(\frac{\cos\phi}{\sin\theta}\right) R_g. \tag{4b}$$

Finally, the flow velocity is estimated as

$$V^2 = U_n^2 + U_e^2 = A_Z^2 + \left(\frac{R_g}{\sin\theta}\right)^2. \tag{5}$$

Hence, the absolute flow offset in the geographical coordinate system, V^2, is equivalent to the absolute flow offset in the slant-range coordinate system projected onto the ground surface. By approximating $U_z = 0$, the flow velocity is not an exact solution, however, the flow velocity calculated by (5) can be used since the ratio of the vertical to the horizontal displacements is considered to be small in the area near the main stream of the Shirase Glacier. Here, the time difference between an image pair of *V* is 14 days (ALOS-2/PALSAR-2 data use). If we assume an error of ±1 pixel in the absolute value of flow velocity, this error becomes ±0.25 km a^{-1} from the mean value of the range or azimuth (minimum) distance and diagonal (maximum) distance of the pixel. Since positions can be practically determined to an accuracy of one-tenth of a pixel (inherent to the offset tracking method), the relative precision level for velocity determination is ±0.03 km a^{-1}.

C. Potential Source of Error in Estimating the Ice Velocity Using PALSAR-2 Data

The estimation of ice flow velocities using an SAR requires consideration of its estimation errors. The major errors are the coregistration error between the image pair and the defocusing and positional offset errors caused by the ionosphere. The error from the coregistrated images in an image pair was coregistrated to be less than 0.1 pixel. Especially the polar observation, it is therefore necessary to consider the effect of the ionosphere on the SAR data.

The propagation path of SAR microwaves until they reach the ground has an ionosphere and an atmospheric layer of approximately 50–1000 km on the surface of the earth. When microwaves pass through the ionosphere, the speed of microwave

$$R\ (u, v) = \frac{\sum_i \sum_j \left[X\,(i, j) - \bar{X}\right]\left[Y\,(i + u, j + v) - \bar{Y}\right]}{\sqrt{\sum_i \sum_j \left[X\,(i, j) - \bar{X}\right]^2}\sqrt{\sum_i \sum_j \left[Y\,(i + u, j + v) - \bar{Y}\right]^2}} \tag{1}$$

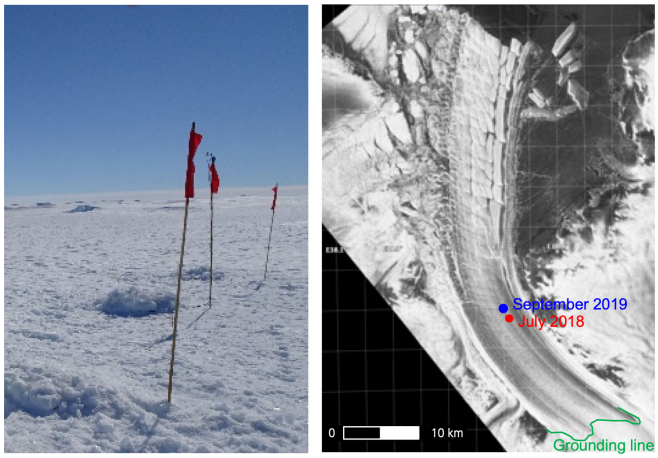

Fig. 3. (a) GNSS receiver of the ApRES where attached the top of the center flag on Shirase Glacier. (b) Position changes of the GNSS receiver of the ApRES at July 2018–September 2019 overlaid the ALOS-2/PALSAR-2 image acquired in 1 July 2018. The grounding line depicted in this figure was derived from [8].

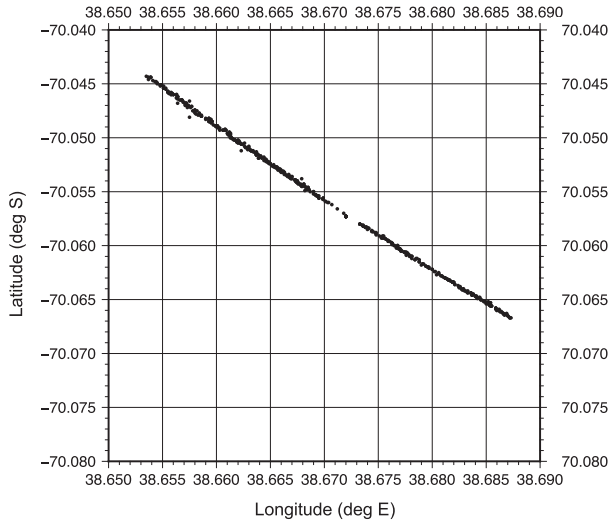

Fig. 4. Trajectory of the ApRES during July 2018–September 2019.

slows down due to the ionospheric total electron content and inversely proportional to the square of the microwave frequency. The properties of the ionosphere are not constant, but vary greatly depending on the difference between day and night, and on the increase in solar activity.

Since the effect of the ionosphere on the offset tracking method using SAR data was considered to appear as an azimuth offset [30], the image pairs that were considered to be affected by the ionosphere will be investigated by calculating the anomaly of 20 pairs of ALOS-2/PALSAR-2 data used in this article. Hence, the validation against some ground truth is indispensable to prove usefulness of this method.

D. ApRES/GNSS Data

The ice flow velocity was measured using the position data from the GNSS receiver on ApRES which was installed at the 20 km downstream from the GL of Shirase Glacier by the helicopter operated the Japan Maritime Self-Defense Force. The GNSS position data was acquired several times a day through the satellite communication service by Iridium communications. Fig. 3 shows a position of ApRES on the Shirase Glacier on July 2018 (start) and September 2019 (end).

E. Measurement of Ice Flow Velocity Using ApRES/GNSS Data

The ice flow velocity was calculated from the distance between the two periods according to the observation time of PALSAR-2. In this article, the distance between two points (s) was determined using the Hubeny's formula [31]. The distance s is calculated as follows:

$$s = \sqrt{(M\Delta\phi)^2 + (N\cos\phi\Delta\lambda)^2} \tag{6}$$

where ϕ is the average latitude between two points, $\Delta\phi$ and $\Delta\lambda$ are the respective differences in latitude and longitude between two points, and M and N are the respective radiuses of the curvature of the meridian and the prime vertical circle. The radiuses of curvature on the ellipsoidal model M and N were calculated as follows:

$$M = \frac{a\left(1-e^2\right)}{\sqrt{\left(1-e^2\sin^2\phi\right)^3}} \tag{7a}$$

$$N = \frac{a}{\sqrt{1-e^2\sin^2\phi}} \tag{7b}$$

where e is the first eccentricity ($\sqrt{1-(b/a)^2}$), and a and b are the semi-major and -minor axes of the earth ellipsoidal model, respectively.

The distance between two points on the earth ellipsoidal model which is set as WGS-84 in this article, is derived by (6). Hence, the distance s with the time difference between SAR observations was converted to annual ice flow velocity.

IV. Results and Discussion

A. Temporal Variation of Flow Velocity From ApRES/GNSS Data

The position data acquired by the ApRES/GNSS receiver is shown in Fig. 4 which is demonstrated the trajectory of the ApRES during 1 July 2018–8 September 2019. The direction of ice flow was approximately 333° in the range of Fig. 4, where a northward heading is defined 0°. The direction of ice flow in this article which was comparable to the previous analysis of JERS-1/SAR data acquired from 1996 to 1998 [32].

Fig. 5 shows the temporal variation of the flow velocity calculated from the ApRES/GNSS position data. This figure also shows the flow velocity over the same period as Fig. 4, with the mean flow velocity of 2.42 km a^{-1}. Since the seasonal mean flow velocity was investigated, this article was defined as the seasons as wintertime from June to August, springtime from September to November, summertime from December and

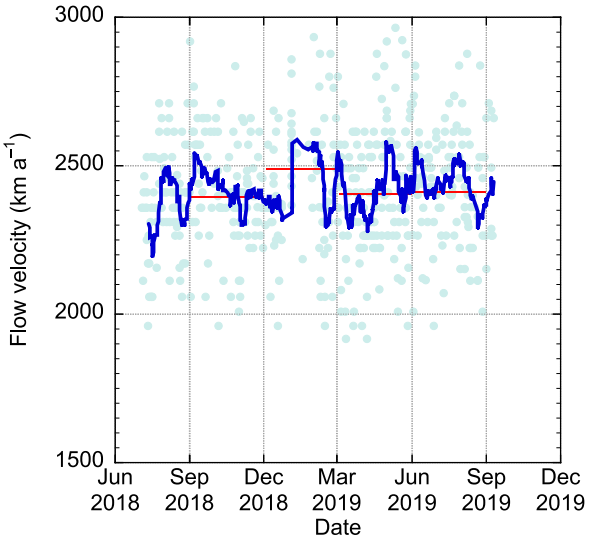

Fig. 5. Temporal variation of flow velocity calculated from the position data acquired by the ApRES/GNSS during July 2018–September 2019. In this figure, cyan plots show measured flow velocities and the blue and red lines shows their 14-day moving average and seasonal mean, respectively.

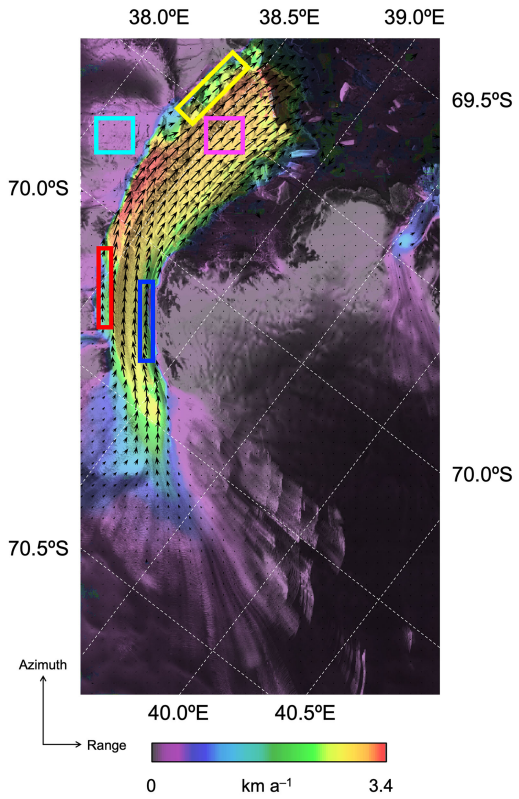

Fig. 6. Spatial distributions of ice velocity for the 20 pairs were calculated by ensemble mean of the velocities at each point. In this figure, the cyan, magenta, yellow, red, and blue frames indicate the areas of mean anomalies extraction (Section IV-B).

January to February, and autumntime from March to May. As a result, flow velocities in wintertime and springtime in 2018 were both 2.40 km a^{-1} and those in summertime, autumntime, and wintertime in 2019 were 2.49, 2.41, and 2.42 km a^{-1}, respectively.

The seasonal variation was calculated as the difference between the flow velocities of summertime and wintertime, and the temporal order in which the wintertime experienced the summertime. The seasonal variation was 0.07 km a^{-1} which was about half of the flow velocity in the downstream region [22]. This is because its location is near the GL, which did not show the similar variation in the flow velocity such as the terminus of the glacier.

B. Anomaly of Flow Velocity

We obtained the spatial distributions of ice flow velocity field for 20 pairs of PALSAR-2 data. Ensemble mean of the velocities at each point revealed an absolute velocity structure of the glacier dynamics, with effectively reducing the short-term error such as an ionospheric delay (Fig. 6). The velocity from each pair, however, contains both dynamical signal of glacier and error component such as an ionospheric effect. Both signal and error have intrinsic spatial scale and characteristics, and hence it is practically effective to derive anomaly from temporal average and to discern the error from signal, given the relatively large number of available pairs. Consequently, we calculated the velocity anomaly by subtracting the mean flow velocity from each of the 20 flow velocities.

Fig. 7 shows the flow velocity field from each 20 pairs of PALSAR-2 data and Fig. 8 shows the anomaly map of the flow velocity. In Fig. 8, the blue color indicates a decreasing trend compared to the mean flow velocity during the analysis period, and the red color indicates an increasing trend, and this figure of (p) and (q), the inverted flow velocity anomalies were found when compared to the adjacent pairs. This might be an effect of the ionosphere because streak-like feature was appeared over the range direction on image and its temporal duration was short enough for observation interval. In order to classify the ionospheric effect, anomalies in regions of the ice sheet and the ice tongue indicated the cyan and magenta frames in Fig. 6, respectively, and extracted each 20 pairs of PALSAR-2 data which are shown in Fig. 9. The mean $\pm$ SD of anomaly in the ice sheet region was –0.01 $\pm$ 0.14 km a^{-1} and that in the glacier region was –0.05 $\pm$ 0.15 km a^{-1}. In the significantly ionospheric affected pairs (Fig. 10), the means of anomaly in the ice sheet region were 0.39 and 0.33 km a^{-1} and those in the glacier region were 0.25 and –0.52 km a^{-1}. Hence, pairs of (p) and (q) in Fig. 10 were excluded from further discussion in this article, since we considered that the anomaly was larger than SD (approximately $\pm$0.2 km a^{-1}) and was significantly affected by the ionosphere.

Anomalous signals are prominent at the both sides of the glacier streamline, which correspond to the areas of large horizontal shear. The fact that these shear zones reveal high variability is very likely natural given the slight shift in position can lead to a large change. Near the western terminus of Shirase Glacier has a shear zone that is affected by other ice shelves from the west side (yellow frame in Fig. 6), and the mean anomaly for this area is shown in Fig. 11(a). Fig. 11(b) and (c) shows the mean anomalies for the shear zones where the Shirase Glacier

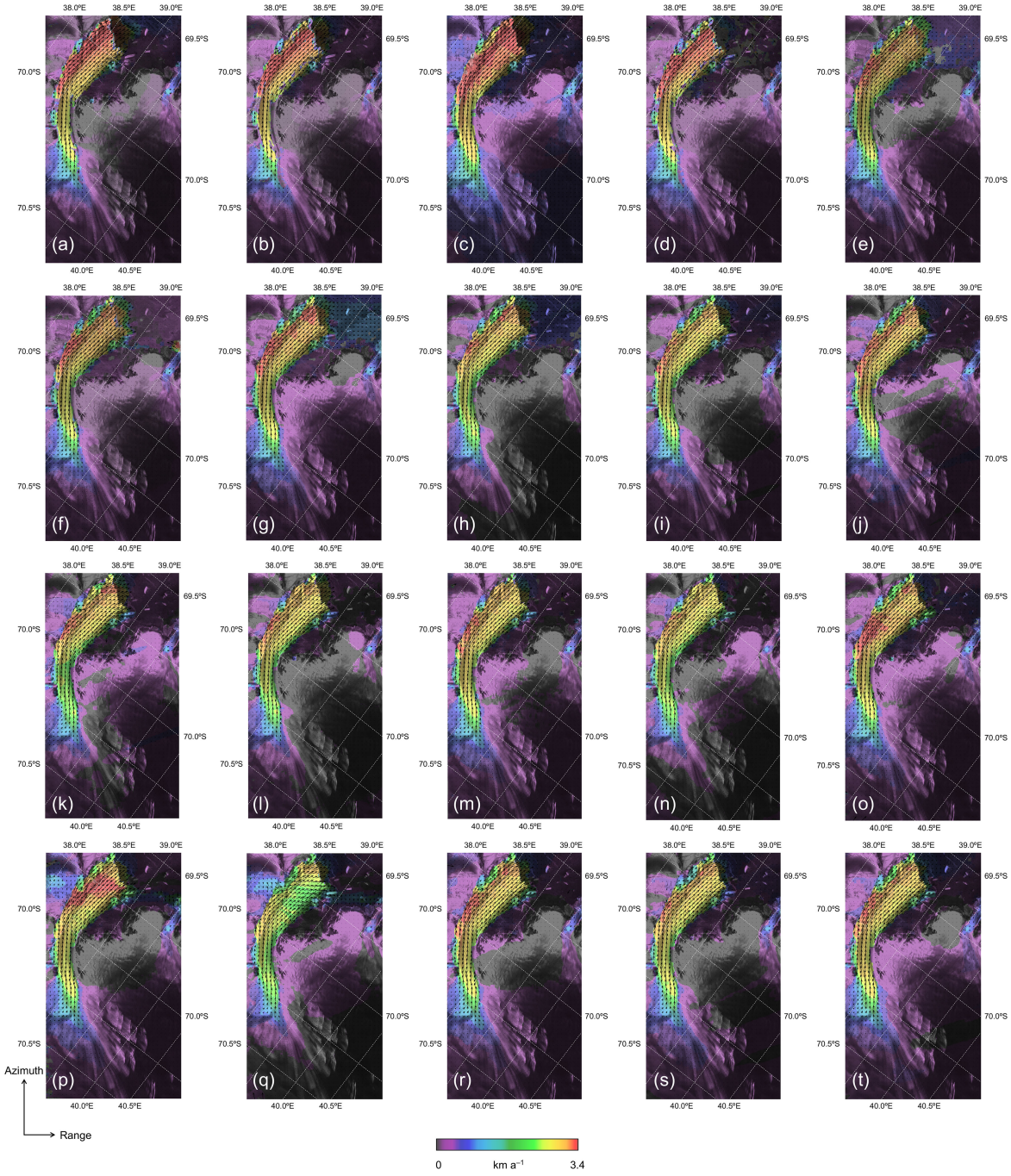

Fig. 7. Map of ice flow velocity field. This figure's labels (a)–(t) correspond to the parenthetical letters of alphabet in Table I.

has contact with exposed rocks on the west and east sides of the glacier (red and blue frames in Fig. 6), respectively.

The mean anomalies in the western terminus of the glacier were –0.09 km a^{-1} in summertime and autumntime and 0.11 km a^{-1} in wintertime and springtime derived from Fig. 11(a). This is because the ice flow in the shear zone at the terminus of Shirase Glacier was suppressed by the accelerated ice flow of the Shirase Glacier in summertime and autumntime, while that flow was released by the deceleration of the ice flow of the glacier in wintertime and springtime. The mean anomalies for the shear zones, where the Shirase Glacier has contact with the western exposed rock, were 0.05 km a^{-1} in summertime and autumntime and –0.23 km a^{-1} in wintertime and springtime derived from Fig. 11(b). Likewise, those with the eastern exposed rock were 0.46 km a^{-1} in summertime and autumntime and –0.66 km a^{-1} in wintertime and springtime derived from Fig. 11(c). As a result, we found that the anomaly change of the shear zone on the west side of the glacier was small, and its change on the east side was large.

Fig. 8. Anomaly map of the flow velocity. This figure's labels (a)–(t) correspond to the parenthetical letters of alphabet in Table I.

The results not only corresponded to the seasonal variation of the flow velocity of the glacier, but also were consistent with the ice flow of the eastern streamline was slower than that of the western streamline of the Shirase Glacier [22].

Here, we consider that the relationship between the asymmetry of flow velocity is in the east and west and the bedrock topography. Although there is not much information on the bathymetry around the Shirase Glacier, the bathymetry of Lützow-Holm Bay and Shirase Glacier was studied by acoustic bathymetry [33]; as a result, the drowned glacial trough which exists, was found to be larger than 1.5-m deep. The bathymetry around the Shirase Glacier is a submerged glacial trough formed

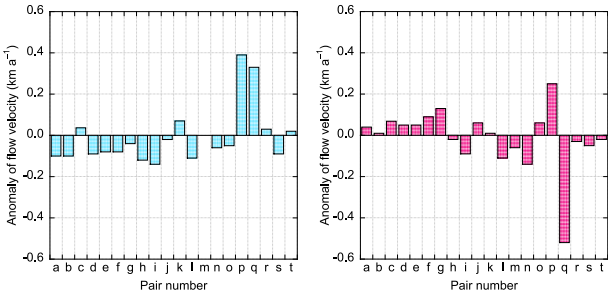

Fig. 9. Mean anomaly derived from (a) ice sheet and (b) ice tongue regions. Each region is shown in Fig. 6. The pair number in this figure is corresponding to the parenthetical letters of alphabet in Table I.

TABLE III
ANNUAL ICE FLOW VELOCITY OF CENTRAL ICE STREAM AT GROUNDING LINE OF SHIRASE GLACIER

Satellite/Sensor	Year	Mean flow velocity
JERS-1/SAR [21]	1996	2.32±0.03 km a^{-1}
	1997	2.32±0.03 km a^{-1}
	1998	2.33±0.03 km a^{-1}
ALOS/PALSAR [22] [23]	2007	2.29±0.02 km a^{-1}
	2008	2.26±0.02 km a^{-1}
	2009	2.25±0.02 km a^{-1}
ALOS-2/PALSAR-2 (ScanSAR) [23]	2014	2.28±0.03 km a^{-1}
	2015	2.28±0.03 km a^{-1}
ALOS-2/PALSAR-2 (Fine beam)	2018	2.32±0.03 km a^{-1}
	2019	2.32±0.03 km a^{-1}

by glacial erosion, and the east side of the drowned glacial trough has the steep slope of 8°–11° with the distinct top of the trough, while the west side has the gentle slope with the asymmetric shape with the indistinct top of the trough. BEDMAP2 [34], a common bedrock topographic map of the Antarctica, shows that areas with bedrock depths below sea level widely cover the Mizuho Plateau, and the free-air anomaly map outlines that the bedrock depth is deeper on the eastern side than on the western side. Furthermore, the basement topography compilation map is compiled by combining ice radar observations from the Japan–Germany Joint Aerial Survey with BEDMAP2 [35]. The results show that the bedrock depth on the west side of the glacier is relatively shallower than that on the east side south of 70°S, which is consistent with the asymmetry of flow velocity in the east–west flow line of the Shirase Glacier.

C. Flow Velocity Profile From SAR Data

To reveal a typical flow structure and its spatiotemporal changes, the ice flow velocity was obtained on the central streamline which was analyzed using the offset tracking method. Table III shows that the annual ice flow velocity at the GL of the Shirase Glacier was studied using SAR images obtained by the JERS-1 in 1996–1998 [21], the ALOS in 2007–2010 [22], [23], and the ALOS-2 in 2014–2015 [23] and 2018–2019 (this article). The annual ice flow velocities have continued largely unchanged over the 24 years since 1996, judging from the ice flow velocities obtained from the JERS-1/SAR, the ALOS/PALSAR, and the ALOS-2/PALSAR-2 observations. The mean ice flow velocity at the GL from 1996 to 2019 was 2.30 km a^{-1}.

TABLE IV
SEASONAL VARIATIONS OF THE FLOW VELOCITIES IN THE DOWNSTREAM, THE GROUNDING LINE, AND THE UPSTREAM REGIONS

Year	Image pair [Summertime – Wintertime]	Downstream region	Grounding line	Upstream region
1997 [23]	[06 Dec 1996 and 19 Jan 1997] – [14 Jul and 27 Aug 1997]	0.10 km a^{-1}	0.00 km a^{-1}	0.13 km a^{-1}
1998 [23]	[06 Jan and 19 Feb 1998] – [18 May and 01 Jul 1998)	0.02 km a^{-1}	–0.02 km a^{-1}	0.07 km a^{-1}
2008 [23]	[27 Dec 2007 and 11 Feb 2008] – [28 Jun and 13 Aug 2008]	0.16 km a^{-1}	0.05 km a^{-1}	0.23 km a^{-1}
2009 [23]	[29 Dec 2008 and 13 Feb 2009] – [16 May and 01 Jul 2009]	0.21 km a^{-1}	0.00 km a^{-1}	0.27 km a^{-1}
2015 [23]	[25 Dec 2014 and 08 Jan 2015] – [28 May and 09 Jul 2015]	0.30 km a^{-1}	0.05 km a^{-1}	0.03 km a^{-1}
2019 This study	[27 Jan and 24 Feb 2019] – [11 and 25 Aug 2019]	0.11 km a^{-1}	0.02 km a^{-1}	0.03 km a^{-1}

The results of applying the offset tracking method to the ALOS-2/PALSAR-2 data to obtain the flow velocities in the central streamline of the Shirase Glacier are shown in Fig. 12. In this figure, the horizontal axis shows the distance from the GL, where the distance from 0 to the left is downstream and the distance from the GL to the right is upstream, and the vertical axis shows the result converted into annual flow velocity. Fig. 8 shows that the flow velocity increases in proportion to the flow distance from the upstream of the Shirase Glacier to the GL position calculated by [8], and the flow velocity at the GL is approximately twice as fast as that at the upstream (30 km from the GL). This trend is similar to that obtained by the JERS-1/SAR and the ALOS/PALSAR [21]–[23], and was considered to have continued for more than 20 years. On the other hand, the flow velocities derived from the JERS-1/SAR and the ALOS/PALSAR in the downstream region (35 km from the GL) showed that the flow velocity is almost constant from the GL to 10 km downstream, and then accelerates again toward the terminus of the floating ice tongue of the Shirase Glacier. While the mean flow velocity derived from the ALOS-2/PALSAR-2 data showed that the flow velocity increased almost linearly from the GL to the downstream.

D. Seasonal Variation of Flow Velocity

Seasonal variations in the flow velocity, where the downstream (from 5 to 35 km downstream from the GL), the GL, and the upstream (from 5 to 30 km upstream from the GL) regions of the Shirase Glacier, were calculated from the flow velocity difference between the summertime and the wintertime with the definition of the temporal order which is the same as Section IV-A. Table IV summarizes the seasonal variations of the flow velocities in the downstream, the GL, and the upstream regions which are also listed the definition of season. The seasonal variations in 2019 were calculated by 0.11, 0.02, and 0.03 km a^{-1} in the downstream region, the GL, and the upstream region, respectively. In Table IV, the seasonal variations in the

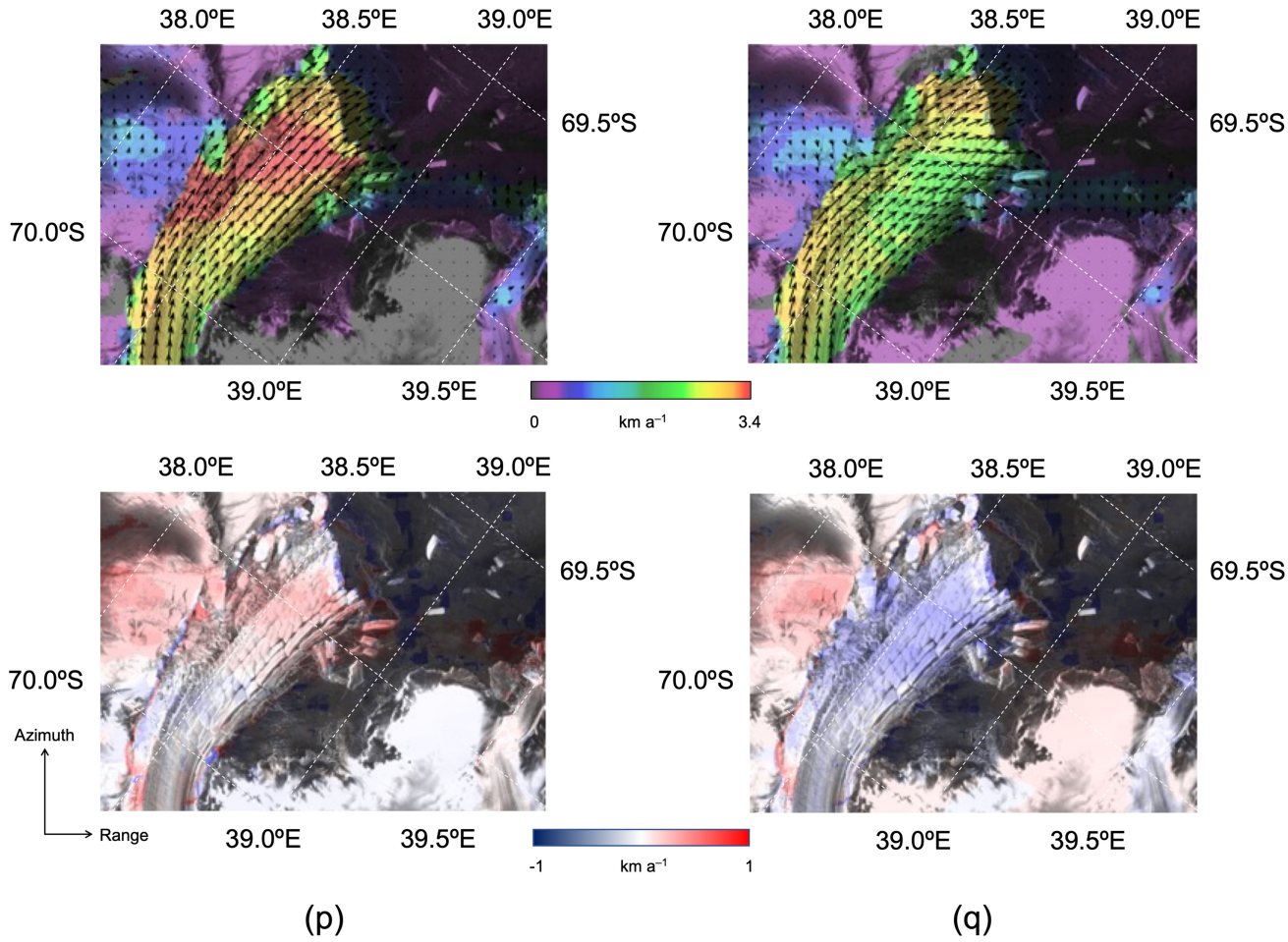

Fig. 10. Extended figure of significantly ionospheric affected pairs whose left figures are (p) and right figures are (q) from Figs. 7 and 8. In this figure, upper figures show a velocity map and bottom figures show an anomaly map.

GL indicated almost no significant while the seasonal variations in the upstream and downstream regions show that the flow velocities in summertime were fast and those in wintertime were slow. Those have tended to be over the 24 years since 1996. The cause of the seasonal variation is still unknown, but given no significant changes in the GL between the upstream and the downstream regions, the two areas can be dominated by different mechanisms.

The seasonal variation varies from year to year. The seasonal variations in 1996–2009 [23] were the upstream region larger than the downstream region, while those in 2015 [23] and 2019 were the upstream region smaller than the downstream region. In 1998, the image pair of wintertime was obtained after the outflow of the floating ice tongue of the Shirase Glacier, and the image pair of wintertime in 2015 was obtained after the breakup of the offshore landfast ice in the Lützow-Holm Bay [23]. In addition, the landfast ice in the bay has repeatedly disintegrated and flown away since 2015 [36], which was considered to accelerate the flow velocity, resulting in small seasonal variations. Therefore, it was inferred that changes in the landfast ice and the floating ice tongue surrounding the glacier were occurred when the seasonal variation was smaller than in previous years.

E. Comparison Between Measured and Estimated Flow Velocity

ALOS-2/PALSAR-2 observations were synchronous with the position data obtained the ApRES/GNSS in 2018–2019, and hence we can compare the measured and estimated ice flow velocities. Fig. 13 shows the result of comparing the ice flow velocity of the Shirase Glacier estimated by the ALOS-2/PALSAR-2 to that measured by the ApRES/GNSS; the correlation coefficient was 0.78 and the RMSE was 0.049 km a^{-1}. Since the effective estimated error of offset tracking method is $\pm$0.03 km a^{-1}, we found that the estimated ice flow velocity applied the offset tracking method to the ALOS-2/PALSAR-2 data was comparable with the measured result by the ApRES/GNSS. Furthermore, the seasonal variations of the error in 2018–2019 were calculated and shown in Table V. As a result, the error was the smallest in the wintertime since the contribution from the surface melting was considered to be negligible and the decorrelation was suppressed in the offset tracking.

When the southernmost landfast ice surrounding these conglomerates disintegrates, the above conglomerate begins to break up as well, releasing icebergs. Thus, the dynamics of the glacier tongue is affected by the stability of the surrounding

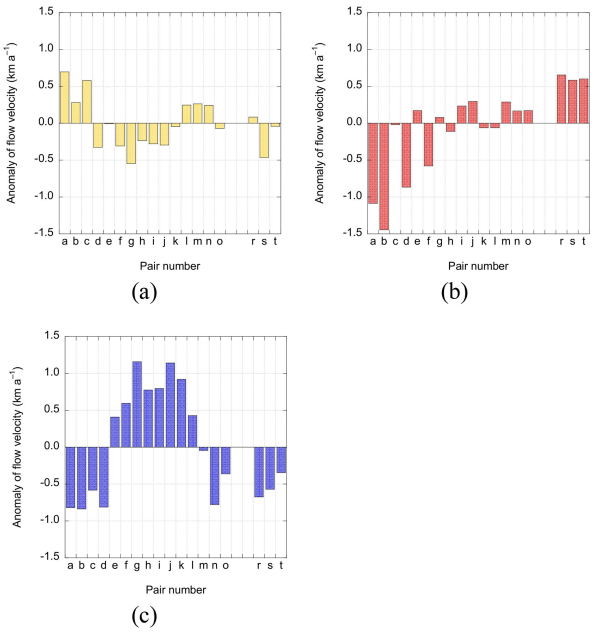

Fig. 11. Mean anomalies derived from the areas of (a) western glacier terminus, the horizontal shear zones contacted with (b) western and (c) eastern exposed rocks. Each region is shown in Fig. 6. The pair number in this figure is corresponding to the parenthetical letters of alphabet in Table I.

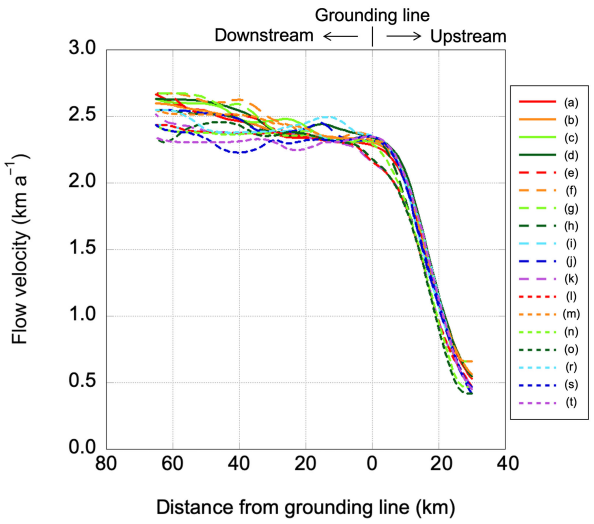

Fig. 12. Variations in flow velocity at the central streamline as a function of distance from the grounding line. Profiles of ice flow estimated in 2018–2019, and the legend of this figure corresponds to Table I. Solid lines indicate those in 2018, dashed lines indicate those in January–May 2019, and dotted lines indicate those in May–September.

TABLE V
SEASONAL VARIATIONS ERRORS DERIVED FROM MEASURED AND ESTIMATED ICE FLOW VELOCITIES

	Image pair	RMSE	Mean	SD
Springtime	(c), (d)	0.049 km a^{-1}	-0.042 km a^{-1}	0.034 km a^{-1}
Summertime	(e) – (i)	0.072 km a^{-1}	0.037 km a^{-1}	0.069 km a^{-1}
Autumntime	(j) – (o)	0.044 km a^{-1}	0.010 km a^{-1}	0.047 km a^{-1}
Wintertime	(a), (b), (r) – (t)	0.017 km a^{-1}	0.002 km a^{-1}	0.019 km a^{-1}

*Image pair of this table corresponds to Table I.

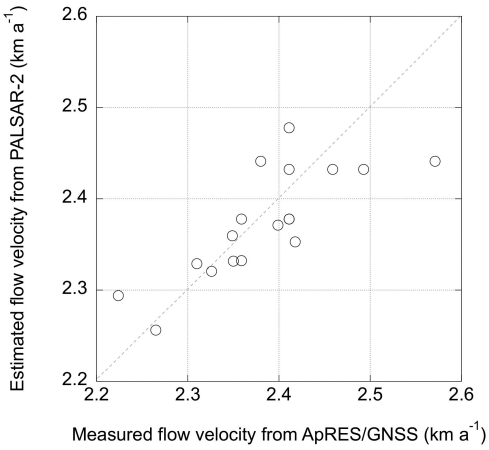

Fig. 13. Comparison between the measured and estimated ice flow velocities from July 2018 to September 2019.

landfast ice in the Lützow-Holm Bay [37]. Large-scale collapse and discharge of landfast ice in the bay has been observed quasi-periodically: for example, in March 1980 [28], January 1988 [23], and May 1998 [38]. In addition to these events, a large part of the glacier tongue also collapsed and was discharged into the bay [21]. More recently, a breakup of landfast ice was observed at the mouth of the Lützow-Holm Bay in March–June 2015, which accelerated the flow velocity of the Shirase Glacier at the GL by approximately 0.1 km a^{-1} [23]. Further collapse and discharge of the landfast ice was observed to extend to the terminus of the glacier in April 2016 [39], and a portion of the glacier tongue was discharged as an iceberg. This is because the seasonal variations of the error through the event of ice flow change may be associated with the condition of landfast ice stability or instability in the Lützow-Holm Bay, but the details of its outlet mechanism remain unknown. Future article of a detailed analysis for the event of the outlet mechanism may allow us to understand the seasonal variations of the error.

V. CONCLUSION

This article showed that temporal variations in ice flow velocities for Shirase Glacier applied the offset tracking method to ALOS-2/PALSAR-2 data. The estimation of ice flow velocities using an SAR requires consideration of its estimation errors, especially the polar observation is necessary to consider the effect of the ionosphere on the SAR data. The image pairs were considered to be affected by the ionosphere investigated by calculating the anomaly. The mean $\pm$ SD of anomaly in the ice sheet region was –0.01 $\pm$ 0.14 km a^{-1} and that in the glacier region was –0.05 $\pm$ 0.15 km a^{-1}. In the significantly ionospheric affected pairs, the means of anomaly in the ice sheet region were 0.39 and 0.33 km a^{-1} and those in the glacier region were 0.25 and –0.52 km a^{-1}. The pairs having large anomaly were larger than SD (approximately $\pm$0.2 km a^{-1}) when pairs were significantly affected by the ionosphere. Hence, the image pairs were excluded from further discussion in this article due to the ionospheric effect.

The annual ice flow velocities have continued largely unchanged over the 24 years since 1996, judging from the ice flow velocities obtained from JERS-1/SAR, ALOS/PALSAR, and ALOS-2/PALSAR-2 observations. The mean ice flow velocity at the GL from 1996 to 2019 was 2.30 km a^{-1}. The seasonal variations in 2019 were calculated by 0.11, 0.02, and 0.03 km a^{-1} in the downstream region, the GL, and the upstream region, respectively. The seasonal variations in the GL indicated almost not significant, while the seasonal variations in the upstream and downstream regions show that the flow velocities in summertime were fast and those in wintertime were slow. Those have tended to be over the 24 years since 1996.

The flow velocity was measured using the GNSS receiver on the ApRES simultaneously with the ALOS-2/PALSAR-2 observation in 2018–2019. As a result of comparing the flow velocity of Shirase Glacier estimated by ALOS-2/PALSAR-2 to that measured by ApRES/GNSS, the correlation coefficient was 0.78 and the RMSE was 0.049 km a^{-1}. Since the effective estimated error of offset tracking method is ± 0.03 km a^{-1}, the estimated flow velocity obtained using the offset tracking method applied to the ALOS-2/PALSAR-2 data which was comparable with the "*in situ*" result by the ApRES/GNSS.

Acknowledgment

ALOS-2's SAR data were provided by the JAXA with the ALOS research announcement (PI No. 1191 and 3049). This work was supported by the Science Program of JARE as Prioritized Research Project (ROBOTICA).

References

[1] Chronological Scientific Tables, National Astronomical Observatory of Japan, Maruzen, Japan, 2006.
[2] Y. Fujii, Y. Ageta, R. Naruse, Y. Ono, H. Fushimi, and T. Shiraiwa, Eds., *Glacier*. Tokyo, Japan: Kokon-Syoin, 1997.
[3] D. G. Vaughan, J. L. Bamber, M. Giovinetto, J. Russell, and A. P. R. Copper, "Reassessment of net surface mass balance in Antarctica," *J. Climate*, vol. 12, no. 4, pp. 933–946, 1999.
[4] E. Rignot, S. Jacobs, J. Mouginot, and B. Scheuchl, "Ice-shelf melting around Antarctica," *Science*, vol. 341, pp. 266–270, 2013.
[5] A. Shepherd and D. Wingham, "Recent sea-level contributions of the Antarctic and Greenland ice sheets," *Science*, vol. 315, pp. 1529–1532, 2007.
[6] E. Rignot *et al.*, "Recent Antarctic ice mass loss from radar interferometry and regional climate modelling," *Nat. Geosci.*, vol. 1, pp. 106–110, 2008.
[7] D. J. Drewry, S. R. Jordan, and E. Jankowski, "Measured properties of the Antarctic ice sheet: Surface configuration, ice thickness, volume and bedrock characteristics," *Ann. Glaciol.*, vol. 3, pp. 83–91, 1982.
[8] K. Nakamura, T. Yamanokuchi, K. Doi, and K. Shibuya, "Net mass balance calculations for the Shirase drainage basin, East Antarctica," *Polar Sci.*, vol. 10, no. 2, pp. 111–122, 2016.
[9] D. Hirano *et al.*, "Strong ice-ocean interaction beneath Shirase Glacier tongue in East Antarctica," *Nat. Commun.*, vol. 11, pp. 4221–4221, 2020.
[10] R. Naruse, "Studies on the ice sheet flow and local mass budget in Mizuho Plateau, Antarctica," *Contributions Inst. Low Temp. Sci., Hokkaido Univ., Ser. A*, vol. 28, pp. 1–54, 1978.
[11] K. Shibuya and K. Ito, "On the flow velocity of the ice sheet along the traverse route from Syowa to Mizuho stations, East Antarctica," *Memoirs Nat. Inst. Polar Res. Special Issue*, vol. 28, pp. 260–276, 1983.
[12] O. Ootaki and S. Fujiwara, "Measurement of ice sheet movement at S16, East Antarctica, using GPS," *Polar Geosci.*, vol. 11, pp. 9–13, 1998.
[13] R. M. Goldstein, H. Engelhardt, B. Kamb, and R. M. Frolich, "Satellite radar interferometry for monitoring ice sheet motion: Application to an Antarctic ice stream," *Science*, vol. 262, pp. 1525–1530, 1993.
[14] T. Ozawa, K. Shibuya, K. Doi, and S. Aoki, "Detection of grounding line and vertical displacement of ice shelf by SAR interferometry—A case study for the Stanjukovicha ice shelf, East Antarctica, using ERS tandem SAR data," *Polar Geosci.*, vol. 15, pp. 112–122, 2002.
[15] T. Yamanokuchi, K. Doi, and K. Shibuya, "Validation of grounding line of the East Antarctic ice sheet derived by ERS-1/2 interferometric SAR data," *Polar Geosci.*, vol. 18, pp. 1–14, 2005.
[16] T. Ozawa, K. Doi, and K. Shibuya, "Detection of ice flow and deformation of the Antarctic ice sheet using JERS-1 SAR interferometry," *J. Geodetic Soc. Jpn.*, vol. 46, no. 1, pp. 43–52, 2000.
[17] M. Nakawo, Y. Ageta, and A. Yoshimura, "Discharge of ice across Soya Coast," *Memoirs Nat. Inst. Polar Res. Special Issue*, vol. 7, pp. 235–244, 1978.
[18] Y. Fujii, "Aerophotographic interpretation of surface features and estimation of ice discharge at the outlet of the Shirase drainage basin, Antarctica," *Antarctic Rec.*, vol. 72, pp. 1–15, 1981.
[19] F. Pattyn and D. Derauw, "Ice-dynamic conditions of Shirase Glacier, Antarctica, inferred from ERS SAR interferometry," *J. Glaciol.*, vol. 48, no. 163, pp. 559–565, 2002.
[20] E. Rignot, "Mass balance of East Antarctic glaciers and ice shelves from satellite data," *Ann. Glaciol.*, vol. 34, pp. 217–227, 2002.
[21] K. Nakamura, K. Doi, and K. Shibuya, "Estimation of seasonal changes in the flow of Shirase Glacier using JERS-1/SAR image correlation," *Polar Sci.*, vol. 1, no. 2–4, pp. 73–83, 2007.
[22] K. Nakamura, K. Doi, and K. Shibuya, "Fluctuations in the flow velocity of the Antarctic Shirase Glacier over 11-years period," *Polar Sci.*, vol. 4, no. 3, pp. 443–455, 2010.
[23] K. Nakamura, T. Yamanokuchi, S. Aoki, K. Doi, and K. Shibuya, "Temporal variations in the flow velocity for Shirase Glacier in Antarctica over a 20-year period," *Seppyo*, vol. 79, no. 1, pp. 3–15, 2017.
[24] M. Tobita, S. Fujiwara, M. Murakami, H. Nakagawa, and P. A. Rosen, "Accurate offset estimation between two SLC images for SAR interferometry," *J. Geodetic Soc. Jpn.*, vol. 45, no. 4, pp. 297–314, 1999.
[25] T. Kobayashi, M. Tobita, and M. Murakami, "Pixel offset technique for measuring local large ground surface displacement," *J. Geodetic Soc. Jpn.*, vol. 57, no. 2, pp. 71–81, 2011.
[26] R. Naruse, "Surface flow and strain of the ice sheet measured by a triangulation chain in Mizuho Plateau," *Memoirs Nat. Inst. Polar Res. Special Issue*, vol. 7, pp. 198–226, 1978.
[27] S. Mae and R. Naruse, "Possible causes of ice sheet thinning in the Mizuho Plateau," *Nature*, vol. 273, pp. 291–292, 1978.
[28] Y. Fujii, *Science in Antarctica*, vol. 4. Tokyo, Japan: Kokon-Shoin, 1982.
[29] M. Muto and M. Furuya, "Surface velocities and ice-front positions of eight major glaciers in the Southern Patagonian ice field, South America, from 2002 to 2011," *Remote Sens. Environ.*, vol. 139, pp. 50–59, 2013.
[30] A. L. Gray, D. E. Mattar, and G. Sofko, "Influence of ionospheric electron density fluctuations on satellite radar interferometry," *Geophys. Res. Lett.*, vol. 27, no. 10, pp. 1451–1454, 2000.
[31] M. Takasaki, *Cartography*, vol. 3. Tokyo, Japan: Asakura-Shoten, 1994.
[32] K. Nakamura, K. Doi, and K. Shibuya, "Why is Shirase Glacier turning its flow direction eastward?," *Polar Sci.*, vol. 1, no. 2–4, pp. 63–71, 2007.
[33] K. Moriwaki and Y. Yoshida, "Submarine topography of Lützow-Holm Bay, Antarctica," *Memoirs Nat. Inst. Polar Res. Special Issue*, vol. 28, pp. 247–258, 1983.
[34] P. Fretwell *et al.*, "BEDMAP2: Improved ice bed, surface and thickness datasets for Antarctica," *Cryosphere*, vol. 7, pp. 375–393, 2013, doi: 10.5194/tc-7-375-2013.
[35] Y. Nogi, W. Jokat, K. Kitada, and D. Steinhage, "Geological structures inferred from airborne geophysical surveys around Lützow-Holm Bay, East Antarctica," *Precambrian Res.*, vol. 234, pp. 279–287, 2013.
[36] K. Nakamura, S. Aoki, T. Yamanokuchi, T. Tamura, S. Ushio, and K. Doi, "Fluctuations of the ice flow velocity of Shirase Glacier and its surrounding landfast ice displacement in East Antarctica derived from ALOS-2/PALSAR-2 image correlation," in *Proc. IEEE Int. Geosci. Remote Sens. Symp.*, 2019, pp. 4172–4174.
[37] S. Ushio, H. Wakabayashi, and F. Nishio, "Sea ice variation in Lu¨tzow–Holmbukta, Antarctica, during the last fifty years," *Seppyo*, vol. 68, pp. 299–305, 2006.
[38] H. Enomoto, F. Nishio, H. Warashina, and S. Ushio, "Satellite observation of melting and break-up of fast ice in Lützow-Holm Bay, East Antarctica," *Polar Meteorol. Glaciol.*, vol. 16, pp. 1–14, 2002.
[39] S. Aoki, "Breakup of land-fast sea ice in Lu¨tzow-Holm Bay, East Antarctica, and its teleconnection to tropical Pacific Sea surface temperatures," *Geophys. Res. Lett.*, vol. 44, pp. 3219–3227, 2017.

Kazuki Nakamura (Member, IEEE) received the B.E. degree in integrated arts and sciences, and the M.E. degree in education from the Hokkaido University of Education, Hokkaido, Japan, in 1998 and 2000, respectively, and the Ph.D. degree in science from the Chiba University, Chiba, Japan, in 2003.

He was a Postdoctoral Fellow in remote sensing science with the Communications Research Laboratory (currently, the National Institute of Information and Communications Technology), Koganei, Japan, from 2003 to 2006, and the National Institute for Polar Research, Itabashi (currently, Tachikawa), Japan, from 2006 to 2007. In 2007–2012, he was a Postdoctoral Fellow in remote sensing science with the National Institute of Advanced Industrial Science and Technology, Tsukuba, Japan. Since 2012, he has been with the College of Engineering, Nihon University, Koriyama, Japan, where he is currently an Associate Professor with the Department of Computer Science. His research interests include microwave remote sensing of sea–ice, glacier, and various targets of the earth.

Dr. Nakamura is a member of AGU, the International Glaciological Society, the Remote Sensing Society of Japan, the Japanese Society of Snow and Ice, and the Japan Society of Civil Engineers.

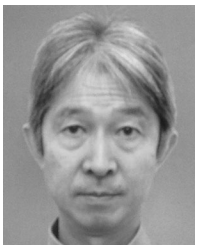

Shigeru Aoki received the B.E. and M.E. degrees in geophysics from the Kyoto University, Kyoto, Japan, in 1990 and 1992, respectively, and the Ph.D. degree in science from the Kyushu University, Fukuoka, Japan, in 1995.

He was a Postdoctoral Fellow in physical oceanography with the Japan Society for the Promotion of Science, Tokyo, Japan, in 1995, and a Research Associate with the National Institute for Polar Research, Itabashi (currently, Tachikawa), Japan, from 1995 to 2003. Since 2003, he has been an Associate Professor with the Institute of Low Temperature Science, Hokkaido University, Hokkaido, Japan. His research interests include physical oceanography and climate change in the Southern Ocean and Antarctica.

Tsutomu Yamanokuchi received the B.S. degree in astrophysics from the Nagoya University, Nagoya, Japan, in 1993, the M.S. degree in oceanography from the Kyushu University, Fukuoka, Japan, in 1995, and the Ph.D. degree in polar science from the Graduate University for Advanced Studies, Tokyo, Japan, in 2007.

He joined the Remote Sensing Technology Center of Japan, in 1995, where he is an in-charge of SAR data applications. Since 2018, he has been a Visiting Associated Professor with the Chiba University, Chiba, Japan. His research interests include applications of SAR data, particularly to retrieve geophysical parameters on cryosphere by InSAR techniques.

Takeshi Tamura received the B.S. degree in science and the M.S. and Ph.D. degrees in environmental earth science from the Hokkaido University, Sapporo, Japan, in 2001, 2003, and 2007, respectively.

He was an Honorary CRC Fellow with the Antarctic Climate and Ecosystems Cooperative Research Centre, University of Tasmania, Hobart, TAS, Australia, from 2010 to 2011. Since 2011, he has been an Assistant Professor (since 2016, an Associate Professor) with the National Institute of Polar Research, Tachikawa, Japan. His research interests include sea–ice and its interaction with ocean, climate system especially for ice–ocean interaction, and microwave remote sensing in polar region.

Koichiro Doi received the Ph.D. degree in science from the Kyoto University, Kyoto, Japan, in 1993.

He was with the Geospatial Information Authority of Japan, Tsukuba, Japan, from 1992 to 1994, as a Special Researcher for science and technology of the Science and Technology Agency. Since 1995, he has been with the National Institute of Polar Research, Tachikawa, Japan. His research interests include interaction between ice sheet mass change and the solid earth using geodetic observations including satellite remote sensing.